PNAS
www.pnas.org

Supplementary Information for

B cells migrate into remote brain areas and support neurogenesis and functional recovery after focal stroke in mice

Sterling B. Ortega[a,b,c,1], Vanessa O. Torres[b,c,1], Sarah E. Latchney[d], Cody W. Whoolery[d], Ibrahim Z. Noorbhai[b,c], Katie Poinsatte[b,c], Uma M. Selvaraj[b,c], Monica A. Benson[b,c], Anouk J. M. Meeuwissen[b,c], Erik J. Plautz[b,c], Xiangmei Kong[b,c], Denise M. Ramirez[b,c], Apoorva D. Ajay[b,c], Julian P. Meeks[b,c,e], Mark P. Goldberg[b,c], Nancy L. Monson[b,c], Amelia J. Eisch[d,f,g], and Ann M. Stowe[b,c,h,2]

[1] denotes equal contribution

[a]Department of Pathology, University of Iowa, Iowa City, IA 52242; [b]Department of Neurology and Neurotherapeutics, UT Southwestern Medical Center, Dallas, TX 75390; [c]Peter O'Donnell, Jr. Brain Institute, UT Southwestern Medical Center, Dallas, TX 75390; [d]Department of Psychiatry, UT Southwestern Medical Center, Dallas, TX 75390; [e]Department of Neuroscience, UT Southwestern Medical Center, Dallas, TX 75390; [f]Department of Neuroscience, Perelman School of Medicine, University of Pennsylvania, Philadelphia, PA 19104; [g]Department of Anesthesiology and Critical Care, Children's Hospital of Philadelphia, Philadelphia, PA 19104; and [h]Department of Neurology, University of Kentucky, Lexington, KY 40506

Corresponding author:
Ann Marie Stowe, PhD
Ann.Stowe@uky.edu

www.pnas.org/cgi/doi/10.1073/pnas.1913292117

This PDF file includes:

Supplementary Materials and Methods
Figures S1 to S6
SI References

Material and Methods

Transient middle cerebral artery occlusion: Animals were anesthetized (2% isoflurane/ 70% NO_2/ 30%O_2), body temperature maintained 37ºC, and left middle cerebral artery (MCA) exposed for transcranial Laser Doppler flowmetry (TSI, Inc) according to previously published methods (1-4). A blunted suture (6.0-gauge nylon, 12 mm) was advanced to block the MCA (>80% reduction relative to baseline blood flow) by surgeons blinded to condition, between 8-14:00 hours, with 10 mice/surgeon/day maximum, with minimum of 2 duplicate experimental days for each outcome measure. All surgical data, including inclusion/exclusion numbers are available upon request and summarized in the Methods section of the main text. Animals were placed in an incubator (34ºC), re-anesthetized after 60 minutes, and suture withdrawn. Flowmetry confirmed reperfusion (CBF >50% baseline). Animals were monitored and those not meeting blood flow criteria will be removed. Neurological deficit was scored on an established scale of 0-4 (1).

***In vitro* and *In vivo* Infarct Volume Assessment:**

Cresyl violet/stereology: Brains were extracted and cryoprotected by immersion in 15% sucrose solution for 24 hr, followed by immersion in 30% sucrose solution until sectioning. Coronal sections (40 um) were serially cut on a freezing microtome and stained with cresyl violet (5). 40x digital images of the slides were obtained using whole slide imaging (Nanozoomer 2.0HT, Hamamatsu Photonics, Hamamatsu-shi, Japan). Infarct volumes were quantified by a blinded observer in Stereo Investigator stereology software (Microbrightfield Biosciences, Williston, VT) using the Cavalieri Estimator Probe, which calculates an estimation of a volume in a user-defined region of interest. Infarcted tissue was defined as areas with pyknotic cells.

TTC: For infarct volume assessment, animals were perfused, brains removed and sectioned into 1.0 mm thick coronal sections. Brains were then placed in 2,3,5-Triphenyl Tetrazolium Chloride (TTC) solution, which demarcates mitochondrial dysfunction, an indicator of neuropathology, and quantified by an observer blinded to experimental treatment using Image J software (NIH, v1.47f) (1, 6).

MRI: For the *in vivo* infarct volume assessment, magnetic imaging resonance (MRI) was conducted using a 7-Tesla small animal MRI system (Agilent (Varian) Inc., Palo Alto, CA) with a 40 mm. Millipede coil and a 400mT/m gradient coil set. Under anesthesia (1-2% isoflurane/ 70% NO_2/ 30%O_2), animals were placed supine with respiratory sensor head first and centered with respect to the center of a RF coil. Through the imaging session, animals were monitored for respiration rate (SA Instruments, Stony Brook NY). For volume measurements of brain, high-resolution T_2-weighted fast spin echo (FSE) axial images were acquired on the entire brain. The imaging parameters were: TR/TE = 2500/60 msec., FOV = 25.6x25.6 mm., matrix size = 256x256, slice thickness = 1 mm., no gap, 8 averages, affording 100 µm. in-plane resolution and a total scan time of 10 minutes and 45 seconds. Hyper-intense areas, reflecting high content of water, such as edema and dilated/expanded ventricles, were calculated on the selected T_2-weighted images by manual segmentation using ImageJ.

The calculated hyper-intense areas were multiplied by slice thickness (1 mm.), for a total of 15 slices, to obtain total volume of injury.

B cell isolation and intravenous injection: Using magnetic B cell isolation kits (STEMCELL), donor B cells were isolated from spleens of naïve adult male C57Bl/6J (Jackson Labs) mice or hCD20- transgenic mice. $5x10^6$ B cells were labeled with a fluorescent proliferation dye (e450; eBioscience) and intravenous injected into recipient mice and sacrificed according to timelines shown in Fig. 1. Peripheral migration of B cells into spleen and cervical lymph nodes was assessed using flow cytometry. Brains were extracted and further postfixed overnight in 4% PFA at 4 °C, transferred to PBS + 0.01% sodium azide and stored at 4 °C until embedding.

Flow cytometry: A general leukocyte survey was performed on cells from the spleen, processed into a single cell suspension and $1x10^6$ bulk cells were used for quantification using fluorescent antibodies specific to leukocytes (CD45-APC-Cy7), B cells (CD19-Alexa 700), monocytes/macrophages (CD11b-PE), neutrophils (GR1-FITC), NK cells (NK1.1-Percp 5.5), and T cells (TCR-PE-Cy5; CD4-PacBlue). Cells were incubated for 30 min. at 4°C and subsequently washed and fixed in 1% paraformaldehyde (Electron Microscopy Science, Harfield PA). Flow cytometric data were acquired using a BD FACS Canto using FACS Diva 6.0 software. FlowJo 9.0 software (Tree Star, Ashland, OR) was used to subset leukocytes according to gating strategy.

Mixed Cortical Cultures: Cortical and hippocampal tissue from postnatal day 0-2 YFP2.2 or C57Bl/6J pups was digested using 0.25% Trypsin-EDTA (Hyclone) to isolate cells to be plated at density of $1.8\text{-}2.0x10^6$ cells per well in a 6-well culture dish in mixed cortical media (1x DMEM (Corning), 10% fetal bovine serum (Gemini), 1% sodium pyruvate (Corning), and 100µg/mL Primocin (InvivoGen)) until confluent (minimum 7 days). Naïve B cells were isolated via negative selection EasyStep magnetic beads (Miltenyi Biotec) from spleens of adult 8-12 week old male C57BL/6 mice. For B cell pre-treatment, B cells were co-cultured for 4 days prior to oxygen-glucose deprivation (OGD) in 0.05:1.0, 0.1:1.0, or 1.0:1.0 B cell:CNS cells ratios. In B cell post-treatment, B cells were co-cultured for 4 days immediately after OGD. OGD was induced for 2 hours by exposure to 0.1% O_2 in a hypoxic chamber with serum/glucose-free HBSS (Cellgro). Following a 3-day post-OGD recovery, neuronal protection was assessed using MAP2+ immunofluorescent staining, and confocal microscopy (Zeiss LSM 880 Inverted microscope, 10x, 4 images/well). Cells per image were quantified using the counter tool in Photoshop CS6, normalized to non-B cell control, and analyzed by one-way ANOVA, Bonferroni post-hoc (Graph-pad Prism7).

Sample Preparation for Serial Two-photon Tomography: B cell migration into the brain was assessed using 3D serial two-photon tomography (STPT)(7) of the entire brain volume (TissueCyte 1000 microscope, TissueVision, Cambridge, MA). To prepare samples for STPT, a 4.5% (w/v) agarose (Type 1A, low EEO, Sigma Catalog #A0169) solution in 50 mM phosphate buffer was prepared and oxidized by adding 10 mM $NaIO_4$ (Sigma Catalog #S1878) and stirring gently for 2 to 3 hours in the dark. The agarose solution was filtered with vacuum suction and washed 3 times with 50 mM phosphate buffer. The washed agarose was resuspended in the appropriate volume of phosphate buffer to make a 4.5% agarose solution. The oxidized agarose solution was heated to boiling in a microwave, then transferred to a stirring plate and allowed to cool to 60-65 °C. Brains were embedded by filling a cryoembedding mold (VWR Catalog #15560-215) with oxidized agarose, placing the filled mold on a flat ice pack, and then quickly

submerging the brain using forceps into the bottom of the block with the cerebellum touching the bottom of the block (olfactory bulbs facing upward). The agarose block was allowed to fully solidify on a frozen ice pack in the dark. Once the agarose blocks were fully hardened, the agarose blocks including the specimens were removed from the molds and placed in small glass jars, where they were treated overnight at 4 °C in the dark in sodium borohydride buffer (50mM sodium borohydride, 50mM borax, 50mM boric acid, pH 9.0-9.5). After overnight crosslinking, the agarose blocks were transferred to phosphate buffer for storage at 4 °C until TissueCyte imaging. In some samples, a pellet of $e450^{+}$ B cells or unlabeled B cells was embedded next to the brain in the same agarose block in order to provide positive and negative control data for image analysis.

On the day of imaging, agarose blocks containing the brain samples were attached to a custom magnetic slide and with superglue then placed on a magnetized stage within an imaging chamber filled with phosphate buffer. STPT imaging is a block-face imaging technique in which 2-dimensional (2D) mosaic images in the coronal plane are formed near the cut surface of the brain (within ~100 µm of the surface), followed by physical sectioning with a built-in vibrating microtome to cut away the imaged tissue, preparing a new cut surface for imaging (7). For this study, 2D mosaic images were taken at 25, 50, and 75 µm from the cut surface, followed by a vibrating microtome cut at 75 µm (blade vibration frequency of 70 Hz, advancement velocity 0.5 mm/s). This process produced 570 2D mosaic images and 190 physical sections with a lateral resolution of 0.875 µm/pixel (~280 gigabytes of raw data per brain). The excitation laser (MaiTai DeepSee, SpectraPhysics/Newport, Santa Clara, CA) wavelength was 850 nm and was used to excite both YFP and eFluor450. Three image channels of emission fluorescence (pre-set bandpass filters encompassing “red,” “green,” and “blue” fluorophores) were collected with a predetermined photomultiplier tube voltage of 700 V. Individual tiles were adjusted via flat-field correction and stitched into 2D mosaic images of each imaging plane via custom software (“AutoStitcher,” TissueVision) and saved to network-attached storage drives.

TissueCyte Image Analysis: 2D coronal images were transferred to a local computing cluster (“BioHPC”) via 10Gbit network. Custom software written in MATLAB (MathWorks, Natick, MA) was used to normalize intensity across all image (color) channels, forming a 3-color, 3-dimensional (3D) image of each brain. Image stacks were denoised with a 3D median filter for visualization using open-source software tools including Vaa3D (8) and ImageJ/FIJI (9). Additional 3D visualization was facilitated via the ClearVolume plugin (10) for ImageJ/FIJI.

The 3D mouse brain images were registered to Allen Institute for Brain Science Common Coordinate Framework (11) (CCF version 3.0, update October 2017). Specifically, the “red” image channel of each 3D mouse brain image was downsampled to 10 µm square lateral voxels, converted to NIFTI format, then registered to the CCF “average template” (10 µm isotropic voxels). Registration was performed using the "NiftyReg software package (12, 13) using parameters similar to those used in the “aMAP” image analysis pipeline (14). Registration involved 3 main steps: (i) affine registration of experimental mouse brain to CCF average template (via the “reg-aladin” function of NiftyReg) (ii) cubic B-spline transformation (via “reg-f3d”) and (iii) resampling the transformed brains (via “reg-resample”). All 3 color channels were warped to the CCF using the registration information for the “red” color channel. Registered whole brain images were resampled to match pre-registration voxel sizes and converted to 16-bit .tif format for further analysis. These analysis procedures were partially automated using a “nextflow” workflow implemented on the BioHPC cluster.

Interactive, voxel-based supervised machine learning software ("Ilastik"; Reference DOI: 10.1109/ISBI.2011.5872394, https://ieeexplore.ieee.org/document/5872394/) was used to classify image features across the whole mouse brain, including labeled B cells. In brief, maximum intensity projection images of all full-resolution optical planes and color channels within a physical section were created and downsampled to 1.5 µm/pixel lateral resolution (creating a series of 190 3-color images from the 570 optical planes). From these images, 3-5 2D sections spanning the anterior-posterior axis of the brain were chosen for model training. The "Pixel Classification" applet in Ilastik, which implements voxel-based random forest machine learning, was used to interactively classify voxels belonging to five image features ("labels"): black background, tissue autofluorescence, noise (*i.e.* bright voxels resulting from imaging microbubbles in the tissue), injured tissue (characterized by dramatic alterations in the autofluorescence signature found in stroke samples) and blue cells (corresponding to labeled B cells). "Blue cell" classification was performed only on samples in which $e450^+$ B cells had been injected, and were reinforced by training of $e450^+$ B cell pellets embedded in the agarose adjacent to several samples. "Injured tissue" classification was performed only on tissue that had undergone tMCAo. "Autofluorescence," "black background," and "noise" was trained on sections from all experimental conditions. A unified random forest model based on representative images of all conditions was used to assign "probabilities" that each voxel in the whole brain images belonged to each label, resulting in a 5-channel "probability map" for each "label" for each experimental brain. Each 5-channel probability map was finally warped to CCF coordinates as per the above procedures.

A custom MATLAB script was used to quantify the normalized intensity of voxels within all annotated brain region for each of the 5 channels in the "probability map." Normalization was performed by summing the per-channel intensities in each annotated region, then dividing by the total volume in the annotated region. This produced a matrix of normalized intensities for each channel and each annotated region for both hemispheres of the experimental samples. Because the CCF annotation has variable levels of parcellation depending on brain region, macroscopic brain regions of interest (*e.g.*, striatum, hippocampus) were aggregated for simplicity based on the CCF parent/child hierarchical structure.

Rotarod (**Motor Coordination Test):** The rotarod apparatus (IITC Life Science) consists of 5 semi-enclosed lanes and an elevated metal rod (1.25 in dia., 10 in elevation) with a fine textured finish to enhance grip. For each trial, all mice were placed on the unmoving rod, allowed to stabilize their posture, and then rod rotation was initiated. Test parameters were: rotation direction, toward investigator to encourage mice to face away while walking; start speed, 4 rpm; top speed, 44 rpm; acceleration rate, 0.2 rpm/sec (200 sec. from start to top speed); max test duration, 300 sec. Each mouse's trial ended when it either fell from the rod, triggering the fall-detection sensor, or gripped the rod without walking and thereby stayed on the rod for one full rotation (a "passive rotation", in which case the investigator triggered the fall sensor manually). Data was automatically recorded to a computer. Mice that fell within 2 sec. were considered to have been startled by the initial rotation or "off-balance" at the start of the trial, and this data was excluded. Mice underwent 4 trials/day, and the average time from all 4 trials was taken.

Novel object recognition: Each NO and NL task was comprised of three phases (habituation, familiarization, and testing) on separate days. All phases were performed in a blue-squared open-field box (44 x 44 x 30 cm.) under dim light condition (60 lux.)

between 10:00 and 14:00 hours. All mice tested were acclimated in the testing room 1 h. prior to testing. In the NO task, each mouse was habituated in the open-field box without objects for 15 min. each for two days (Days 1 and 2) and locomotor activity was assessed (15). Mice were positioned in the center of the box, and then individual total distance moved during the 15 min. of habituation was automatically recorded using a video tracking system (Noldus Information Technology). In the familiarization phase for NO task (Day 3), mice were subjected to a 1 min. re-habituation to the empty box and then placed in a holding cage. Immediately after, two identical objects (metal cones) were placed near the corners of the box and ~5 cm. from the walls. Mice were returned to the box for familiarization. They were allowed to freely explore until they accumulated a total of 30 sec. exploring both objects. Exploration was defined as the mouse contacting the object with its whiskers, nose, or front paws. We ensured that every mouse spent the same amount of time exploring the objects and avoided any bias due to differences in individual levels of exploration by removing the animal from the box once it had explored the objects for a total of 30 sec. Behaviors such as sitting on the object, looking around, or resting against the object were not counted as exploratory time. Once reaching the 30 sec. criteria, mice were then removed from the box and returned to their home cages. The mice that did not reach criteria within 15 min. were excluded from further testing. In the NO testing phase (Day 4), mice were subjected to a 1 min. re-habituation to the empty box and then placed in a holding cage. Immediately after two objects, one of which was novel (doll) and the other was familiar (metal cone), were placed in the same location as during familiarization, mice were reintroduced into the box, and their exploratory behaviors were recorded by video camera for 10 min., and manually scored later. The position of the object used as novel or familiar in the NO were counter balanced across mice.

Novel location recognition: In the NL task, each mouse was habituated in the open-field box without objects for 15 min. (Day 8). In the familiarization phase for NL task (Day 9), mice were subjected to a 1 min. re-habituation to the empty box then placed in a holding cage. Immediately after, two identical objects (3.5-inch binder clips) were placed in diagonal near the corners of the box (~5 cm from the walls) and mice were returned for familiarization. The mice were allowed to freely explore until they accumulated a total of 30 sec. exploring both objects. Once reaching the 30 sec. criteria, mice were then removed from the box and returned to their home cages. The mice that did not reach criteria within 15 min. were excluded from further testing. In the NL testing phase (Day 10), mice were subjected to a 1 min. re-habituation to the empty box and then placed in a holding cage. Immediately after, the same two identical objects (3.5-inch binder clips), one of which was moved to a NL, were placed near the corners in the box, mice were reintroduced into the box and their exploratory behaviors were recorded by video camera for 10 min. and analyzed later. Time spent exploring each object for 10 min. was scored. To analyze cognitive performance, preference of NO or NL was calculated as time spent exploring the novel object or the familiar object in the novel location divided by the cumulative time spent exploring both objects. The open-field box was cleaned thoroughly with disinfectant solution after each trial to ensure the absence of olfactory cues.

Contextual and cued fear conditioning: Fear conditioning was performed as previously described with slight modifications (16). For fear conditioning training (Day 13), mice were placed in a Plexiglas shock box with clear front and rear walls (MedAssociates) for 2 min., and then a 30 sec., 90 dB acoustic tone co-terminating in a 2 sec., 0.5 mA foot shock was delivered twice with a 1 min. inter-stimulus interval.

Freezing behavior was monitored at 4 sec. intervals by an observer blind to genotype or drug treatment. To test for hippocampal-dependent contextual fear response, mice were placed in the same context 24 h. following training (Day 14) and scored for freezing behavior every 4 sec. for 5 min. To test for hippocampal-independent cued fear response, mice were placed in a novel environment consisting of a Plexiglas floor, a roofed overhead, and a vanilla extract scent (Day 15). Mice were allowed to freely explore for 3 min. followed by a 90 dB acoustic tone for 3 min. Mice were scored for freezing behavior.

Pain sensitivity: To determine whether there was any difference in pain sensitivity between the groups, foot shock sensitivity was measured by delivering a 2 sec. foot shock every 15 sec., starting at 0.05 mA. and increased by 0.05 mA. for each successive foot shock (Day 16). For each mouse, the lowest shock intensity that elicited a flinch, vocalization, or jump was scored.

Immunohistochemistry (IHC): Immediately after the behavior test, all mice were sacrificed with isoflurane overdose and transcardially perfused with 4% paraformaldehyde as described previously (17, 18). All brains were cryoprotected in 30% sucrose with 0.1% sodium azide prior to processing for immunohistochemistry (IHC). 30 µm. coronal sections spanning the entire hippocampus (-0.9 to -3.7 mm from Bregma) were collected at dry ice temperature on a microtome in a 1:6 series to allow for stereological quantification. Hippocampal sections were mounted onto coded superfrost-plus slides (Fisher Scientific) and were allowed to dry for 2 h. (17, 18). After drying, sections were first incubated in 0.01M. citric acid (pH 6.0, 100ºC) for 15 minutes for antigen retrieval. Sections stained for BrdU underwent 2 additional pretreatment steps: permeabilization with trypsin and 0.1% $CaCl_2$ in 0.1M Tris. pH 7.4 (10 min), and denaturation with 2N HCl (30 min.) (18). All slides were then incubated in 0.3% H_2O_2 to quench endogenous peroxidases. Nonspecific binding was blocked with 3% normal donkey serum and 0.3% Triton-X 100 in 1X PBS for 1 h. The following primary antibodies were used: rat monoclonal anti-BrdU (1:400; Accurate) and goat polyclonal anti-DCX (1:500; Santa Cruz Biotechnology). Primary antibody incubation was followed by 2 h. incubation in the appropriate biotin-conjugated secondary antibody and 90 min. in ABC (1:50; Vector Laboratories). $BrdU^+$ and DCX^+ cells were visualized with DAB/metal concentrate (10x; Thermo Scientific). After immunostaining, sections were counterstained with Nuclear Fast Red (Vector Laboratories), dehydrated with graded ethanol, and cover slipped using DPX (Fluka). To minimize variability and add quantification of resulting stains, tissues from all mice in a cohort were processed through IHC simultaneously.

Brightfield microscopic cell quantification: Following IHC on hippocampal sections, unbiased estimates for DCX cell counts were obtained using stereological quantification on an Olympus BX51 System Microscope with a MicroFIRE A/R camera (Optronics) as previously published (17). Estimation of total DCX^+ cell number was performed using the Optical Fractionator Probe within the Stereo Investigator software (MBF Bioscience) according to previously published stereological methods (19). An unbiased counting frame superimposed on the region of interest was used to quantify cell number. Counting was performed using a 40x, 0.63 NA lens. At least 250 cells per mouse were counted, and the average number of counting fields per mouse was close to 300. The average number of sections per mouse counted was 10. To decrease the effect of shrinkage on the tissue, the average measured mounting thickness after processing was approximately 22µm. and we used an optical dissector height of 14µm. The area-

sampling fraction was 1/25 and every 6th section (section sampling fraction) was used to quantify DCX^+ cells within the GCL of the dentate gyrus. The Gunderson coefficient of variance for each mouse quantified was always less than 10%. Data are reported as the total number of DCX^+ cells in the GCL per brain.

BrdU Labeling and Quantification: At the beginning of the neurogenesis studies, all mice received three intraperitoneal (i.p.) injections of bromodeoxyuridine (BrdU; 150mg/kg dissolved in 0.9% saline and 0.007 N NaOH; one injection every 6 h) to label dividing cells in S-phase. (18) Bright field staining of coded slides was visualized with an Olympus BX51 microscope using a 40x, 0.63 NA lens with continuous adjustment through the depth of the section as described previously. (18) Using stereological principles,(17) staining was examined and immunoreactive cells were quantified in the SGZ of the hippocampal dentate gyrus. The SGZ was defined as a region straddling the border of the GCL and the hilus: 30µm into the hilus and the inner half of the GCL adjacent to the hilus (17). Exhaustive counts for $BrdU^+$ cells were undertaken using the optical fractionator method in which every 6th section spanning the entire anterior-posterior hippocampus was examined (-0.6 to -4.8 mm from Bregma). The section sampling fraction was 1/6 and the resulting number of BrdU-positive ($BrdU^+$) cells was multiplied by 6 and reported as total number of cells in the SGZ per brain. Because the raw counts (before multiplication) for the immunoreactive cells counted here were low according to dissector / fractionator standards (20, 21), we used an area sampling fraction of 1 as is commonly used for counting rare cell populations (17) Based on previous work from our laboratory and those of others, (17, 22, 23) the height sampling fraction was set at 1. All cell quantification was done in a blinded fashion.

Granule Cell Layer quantification: Volume estimation of the granule cell layer (GCL) of the dentate gyrus was performed using the Cavalieri Probe within Stereo Investigator as previously described (17). The GCL was viewed and volume determined using an Olympus BX51 microscope with a 10x, NA 0.30 lens. Area sizes from every 6^{th} section were determined using the area measurement tool (based on the Cavalieri estimator) in which an automated grid of test points was superimposed upon the region of interest. The area of the GCL was estimated from the total number of points that fell within the field. To obtain the volume, the sum of the areas measured was multiplied by the sampling fraction (21) and the section thickness (30 µm). The Gunderson coefficient of variance for each mouse quantified was always less than 10%. Data are reported as the total estimated volume (μm^3) of the GCL per brain.

Supplemental Figures:

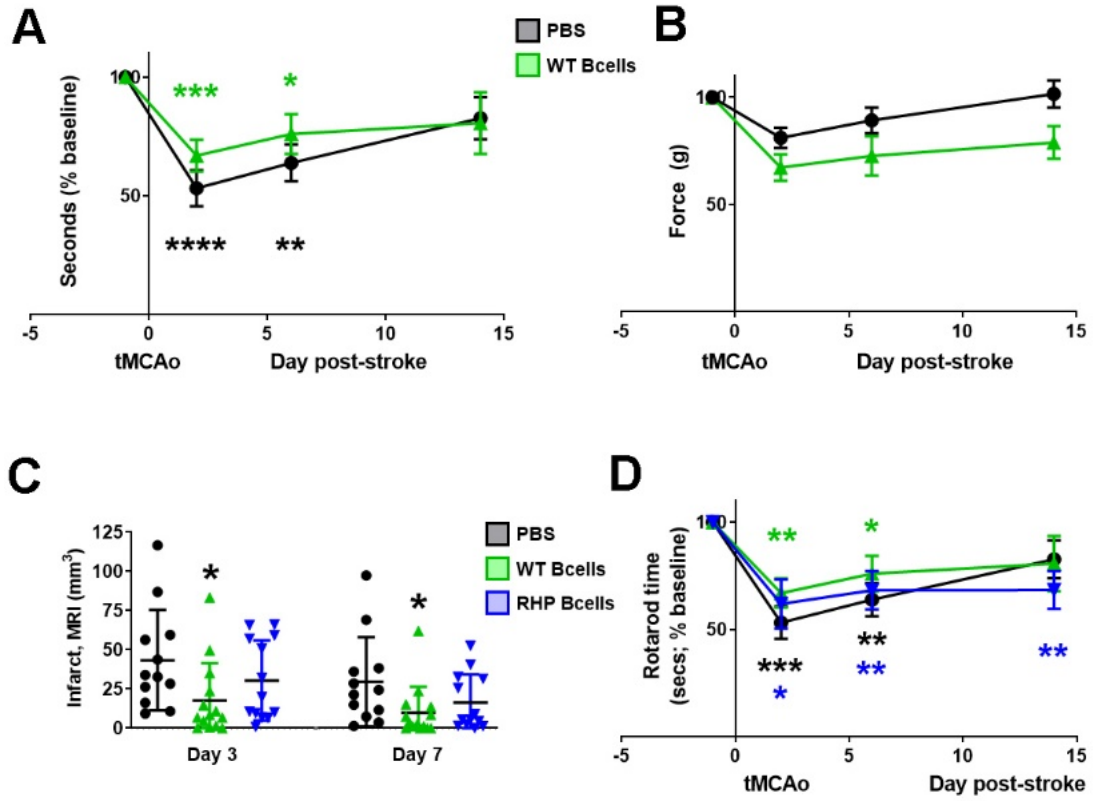

Fig. S1. Rotarod and force grip is unaltered in B cell-treated mice. PBS- and wild type (WT) B cell-treated cohorts exhibited the same rate of recovery as assessed on **(A)** rotarod for motor coordination or **(B)** force grip device for muscle strength. **(C)** Infarct volumes quantified from serial MRI images show that the adoptive transfer of WT B cells (green upward triangles) significantly decreases infarct volumes 3 and 7 days post-stroke, as compared to control PBS (black circles) or repetitive hypoxic preconditioning (RHP)-modulated B cells (downward blue triangles). WT and PBS cohorts are also shown in Figure 1. **(D)** PBS- and WT B cell-treated cohorts exhibited the same rate of recovery as assessed on rotarod (also panel A), while the B(RHP) cell-treated cohort displayed motor deficits that persisted through 2 weeks after tMCAo. A,D: *p<0.05, **p<0.01, ***p<0.001 vs. pre-stroke baseline. C: *p<0.05 vs. PBS.

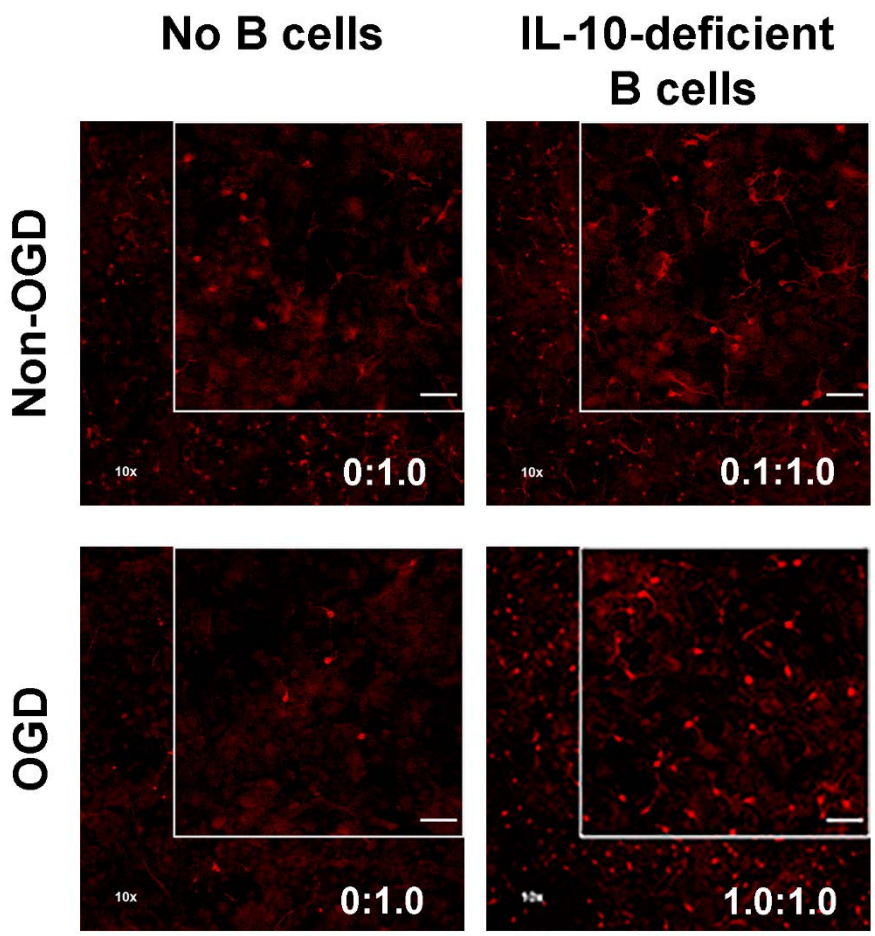

Fig. S2. Representative images of mixed cortical cultures with IL-10-deficient B cells. Panels depict 10X images of microtubule-associated protein $(MAP2)^+$ neurons (red) for treatment (txn) groups shown in Figure 2E,2F, with higher magnification inset. Ratios of B cells to mixed cortical cells are depicted in the lower right corner of each panel for untreated (left images) and IL-10-deficient B cell-treated (right images) groups in both Non-oxygen glucose deprivation (OGD) groups (top panels) and OGD-treated groups (bottom panels). Scale bar = 50 μm

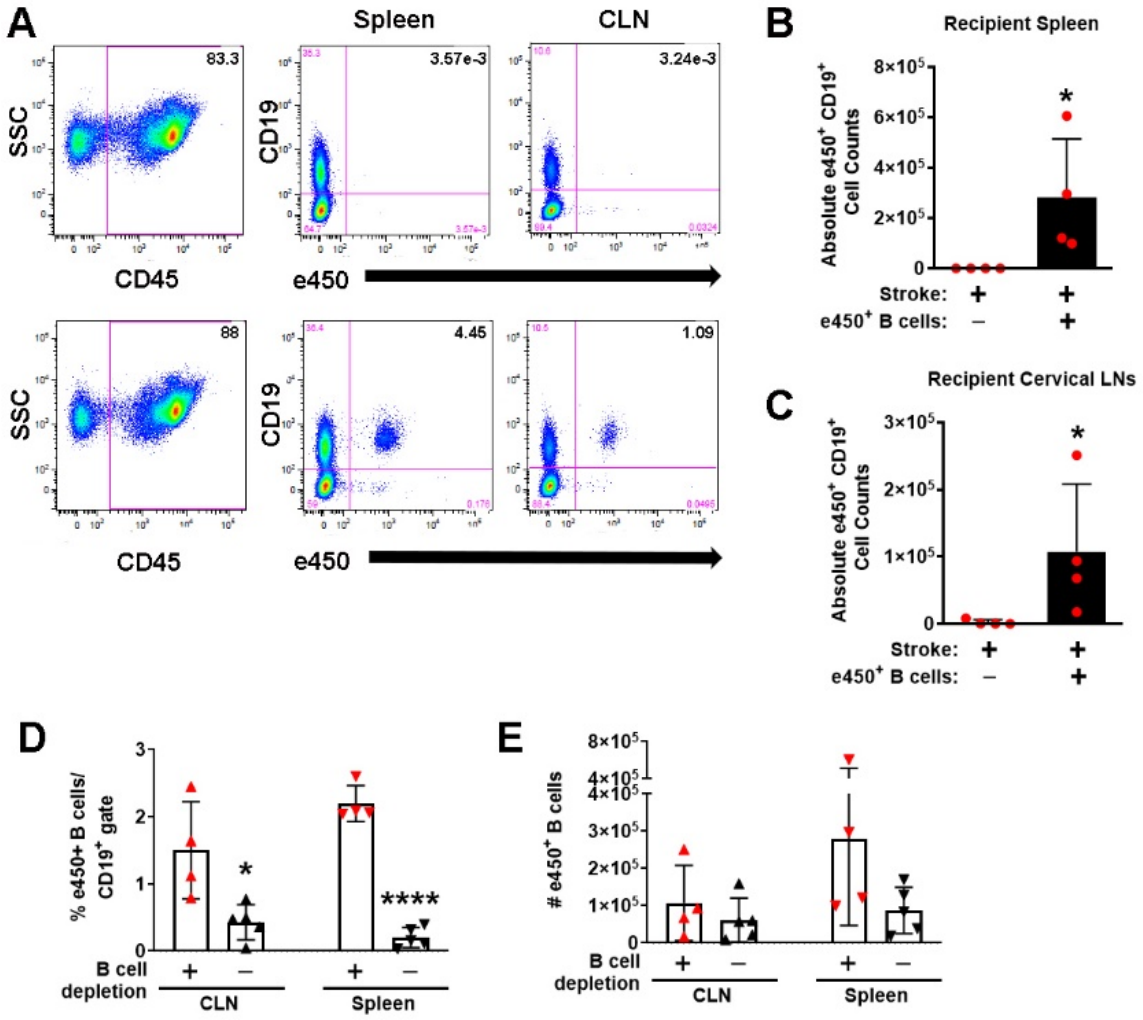

Fig. S3. Confirmation of e450⁺ B cells in systemic circulation. (A) Flow plots from CD45⁺ leukocyte populations (far right plots) for PBS-treated (top row) and e450⁺ B cell-treated (bottom row) mice. CD19⁺ B cells (y axes) labeled with e450 (x axes) are only in the spleens and cervical lymph nodes (CLN) of B cell recipients. Absolute **(B)** splenic and **(C)** CLN counts for e450⁺ B cells in each recipient hCD20⁺ mouse (red circles). **(D, E)** Confirmation of e450⁺ B cells in B cell-depleted mice (red triangles) compared to mice with endogenous B cells (black triangles). While **(D)** percent representation was greatly diminished in the presence of endogenous B cells, **(E)** cell numbers were similar. *p<0.05, ****p<0.0001 compared to B cell-depleted cohort.

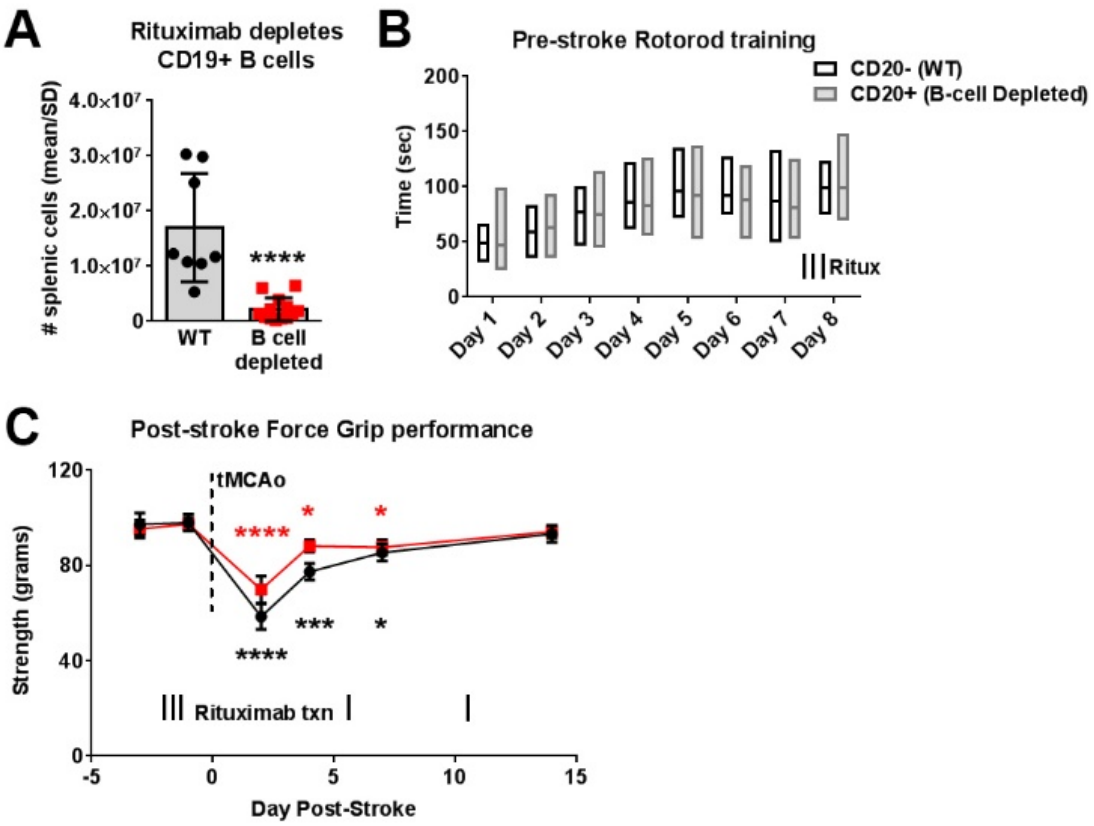

Fig. S4. Genotype does not affect motor learning prior to stroke or muscle strength after stroke. (A) Successfully-depleted $CD20^+$ cells was confirmed by significant reduction of $CD19^+$ cells in the spleen of transgenic human (h)$CD20^+$ transgenic mice (red squares) compared to wild type (WT) littermate controls (black circles). **(B)** $hCD20^+$ mice (i.e. B cell-depleted) and WT $hCD20^-$ mice did not exhibit any differences in motor learning on the rotarod over 8 pre-stroke training sessions. Rituximab (Ritux) was given on the 7^{th} day of training, and two consecutive days over the weekend prior to the 8^{th} day of training. **(C)** Upper extremity force grip was measured for two days prior to transient middle cerebral artery occlusion (tMCAo), then for 4 days post-tMCAo. There was no effect of genotype on the initial loss of grip strength, or subsequent recovery after post-tMCAo, for B cell-depleted mice (red squares) compared to B cell(+) mice (black circles). Mean ± standard deviation (SD) shown. *p<0.05; *** p<0.001; **** p<0.0001.

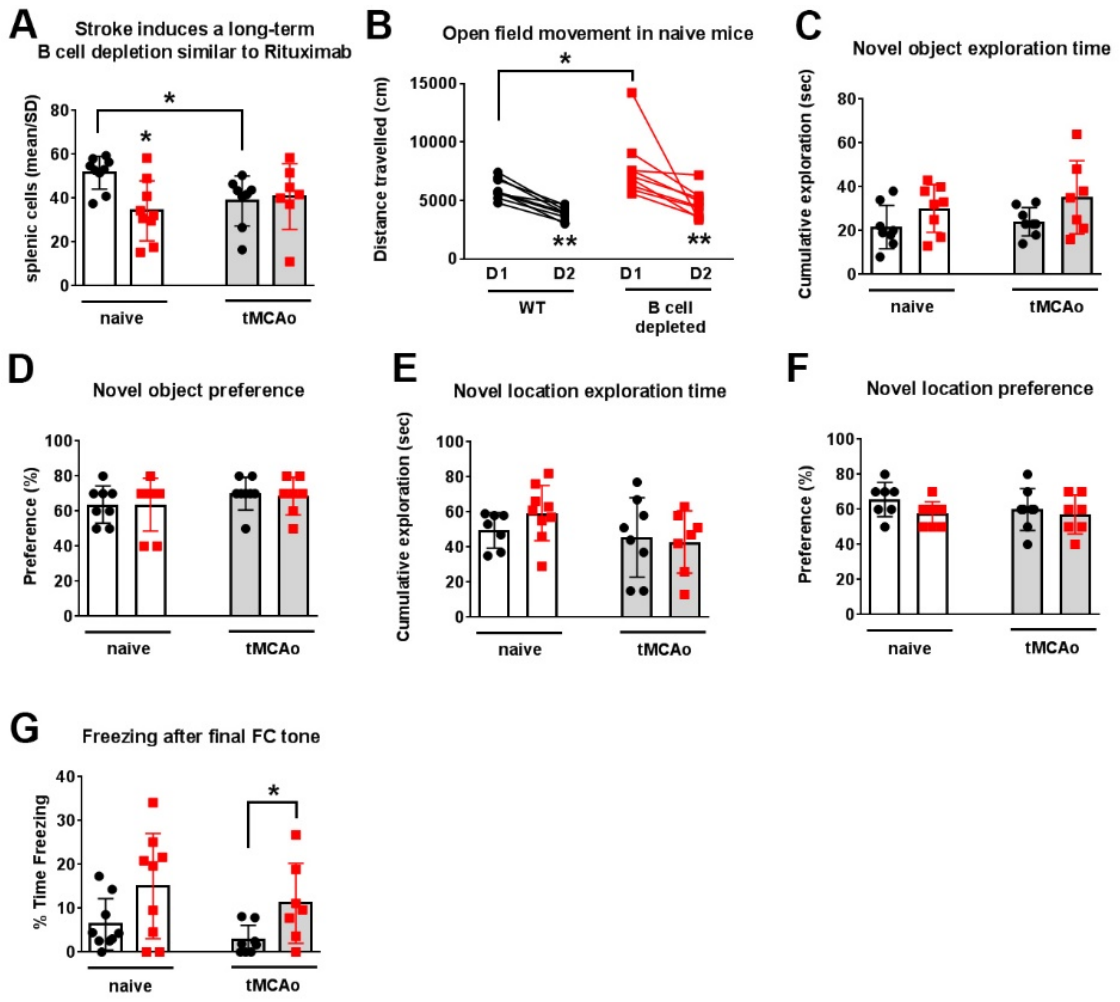

Fig. S5. B cell depletion did not affect non-stressful cognitive function. (A) Rituximab treatment in transgenic human (h)CD20^{+} transgenic mice (red squares) and wild type (WT) littermate controls (black circles) show reductions in B cell representation for both naïve mice and mice that had a transient middle cerebral artery occlusion (tMCAo). **(B-G)** Long-term cognitive function was simultaneously acquired in four cohorts for transgenic human hCD20^{+} mice and littermate hCD20^{-} wild type (WT) mice (black circles) under either healthy, naïve condition (clear bars) or following transient middle cerebral artery occlusion (tMCAo; grey bars). **(B)** Open field movement in naïve mice had a similar day 2 decline as post-tMCAo mice shown in Figure 2. There was a similar response in all four cohorts for the amount of time exploring **(C)** the novel object, as well as **(D)** preference for the novel object. This was also true for cumulative exploration time within the **(E)** novel location, as well as **(F)** preference for the novel location. **(G)** However, on the first day of fear-conditioning, post-stroke B cell-depleted mice exhibited prolonged freezing during the training tones/shocks after the final tone. Mean ± standard deviation (SD) shown. *p<0.05

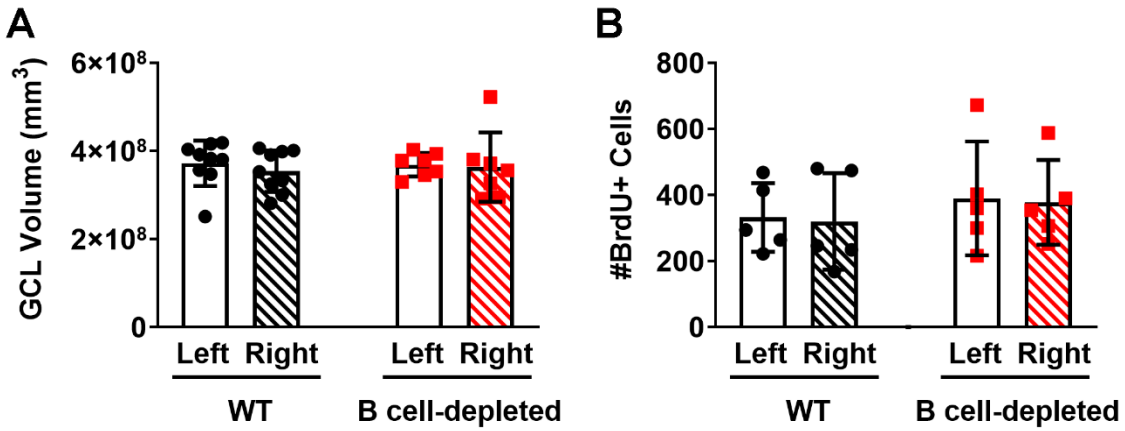

Fig. S6. Long-term B cell depletion in uninjured mice. (A) B cell depletion did not alter granule cell layer (GCL) volume in the dentate gyrus in the absence of stroke, matching neurogenesis data shown in Fig. 7B **(B)** B cell depletion did not affect bromodeoxyuridine $(BrdU)^+$ cells in the dentate gyrus between hemisphere in the absence of stroke. Two-way ANOVA.

References

1. Gidday JM*, et al.* (2005) Leukocyte-derived matrix metalloproteinase-9 mediates blood-brain barrier breakdown and is proinflammatory after transient focal cerebral ischemia. *Am J Physiol Heart Circ Physiol* 289(2):H558-568.
2. Monson NL*, et al.* (2014) Repetitive hypoxic preconditioning induces an immunosuppressed B cell phenotype during endogenous protection from stroke. *J Neuroinflammation* 11:22.
3. Ortega SB*, et al.* (2015) Stroke induces a rapid adaptive autoimmune response to novel neuronal antigens. *Discov Med* 19(106):381-392.
4. Poinsatte K*, et al.* (2015) Quantification of neurovascular protection following repetitive hypoxic preconditioning and transient middle cerebral artery occlusion in mice. *J Vis Exp* (99):e52675.
5. Selvaraj UM*, et al.* (2016) Preconditioning-induced CXCL12 upregulation minimizes leukocyte infiltration after stroke in ischemia-tolerant mice. *Journal of cerebral blood flow and metabolism : official journal of the International Society of Cerebral Blood Flow and Metabolism*.
6. Stowe AM*, et al.* (2009) Neutrophil elastase and neurovascular injury following focal stroke and reperfusion. *Neurobiol Dis* 35(1):82-90.
7. Ragan T*, et al.* (2012) Serial two-photon tomography for automated ex vivo mouse brain imaging. *Nat Methods* 9(3):255-258.
8. Peng H, Ruan Z, Long F, Simpson JH, & Myers EW (2010) V3D enables real-time 3D visualization and quantitative analysis of large-scale biological image data sets. *Nature biotechnology* 28(4):348-353.
9. Schindelin J*, et al.* (2012) Fiji: an open-source platform for biological-image analysis. *Nature methods* 9(7):676-682.
10. Royer LA*, et al.* (2015) ClearVolume: open-source live 3D visualization for light-sheet microscopy. *Nature methods* 12(6):480-481.
11. Oh SW*, et al.* (2014) A mesoscale connectome of the mouse brain. *Nature* 508(7495):207-214.
12. Modat M*, et al.* (2014) Global image registration using a symmetric block-matching approach. *J Med Imaging (Bellingham)* 1(2):024003.
13. Modat M*, et al.* (2010) Fast free-form deformation using graphics processing units. *Comput Methods Programs Biomed* 98(3):278-284.
14. Niedworok CJ*, et al.* (2016) aMAP is a validated pipeline for registration and segmentation of high-resolution mouse brain data. *Nature communications* 7:11879.
15. Cho KO*, et al.* (2015) Aberrant hippocampal neurogenesis contributes to epilepsy and associated cognitive decline. *Nature communications* 6:6606.
16. Powell CM*, et al.* (2004) The presynaptic active zone protein RIM1alpha is critical for normal learning and memory. *Neuron* 42(1):143-153.
17. Latchney SE, Jiang Y, Petrik DP, Eisch AJ, & Hsieh J (2015) Inducible knockout of Mef2a, -c, and -d from nestin-expressing stem/progenitor cells and their progeny unexpectedly uncouples neurogenesis and dendritogenesis in vivo. *FASEB J* 29(12):5059-5071.
18. Latchney SE, Jaramillo TC, Rivera PD, Eisch AJ, & Powell CM (2015) Chronic P7C3 treatment restores hippocampal neurogenesis in the Ts65Dn mouse model of Down Syndrome [Corrected]. *Neurosci Lett* 591:86-92.
19. Latchney SE*, et al.* (2014) Developmental and adult GAP-43 deficiency in mice dynamically alters hippocampal neurogenesis and mossy fiber volume. *Developmental neuroscience* 36(1):44-63.

20. Pakkenberg B & Gundersen HJ (1988) Total number of neurons and glial cells in human brain nuclei estimated by the disector and the fractionator. *Journal of microscopy* 150(Pt 1):1-20.
21. West MJ & Gundersen HJ (1990) Unbiased stereological estimation of the number of neurons in the human hippocampus. *J Comp Neurol* 296(1):1-22.
22. Jayatissa MN, Henningsen K, West MJ, & Wiborg O (2009) Decreased cell proliferation in the dentate gyrus does not associate with development of anhedonic-like symptoms in rats. *Brain Res* 1290:133-141.
23. Eisch AJ, Barrot M, Schad CA, Self DW, & Nestler EJ (2000) Opiates inhibit neurogenesis in the adult rat hippocampus. *Proceedings of the National Academy of Sciences of the United States of America* 97(13):7579-7584.